

# Accelerating Object Detection by Erasing Background Activations

Byungseok Roh<sup>†\*</sup>

Han-Cheol Cho<sup>†</sup>

Myung-Ho Ju<sup>†</sup>

Soon Hyung Pyo

Intel

{peter.roh, han-cheol.cho, lake.ju, sean.pyo}@intel.com

## Abstract

Recent advances in deep learning have enabled complex real-world use cases comprised of multiple vision tasks and detection tasks are being shifted to the edge side as a pre-processing step of the entire workload. However, since running a deep model on resource-constraint devices is challenging, the design of an efficient network is demanded. In this paper, we present an objectness-aware object detection method to accelerate detection speed by circumventing feature map computation on background regions where target objects don't exist. To accomplish this goal, we incorporate a light-weight objectness mask generation (OMG) network in front of an object detection (OD) network so that it can zero out background areas of an input image before being fed into the OD network. The inference speed, therefore, can be expedited with sparse convolution. By switching background areas to zeros for entire activations, the average number of zero values on MobileNetV2-SSDLite with ReLU activation is increased further, from 36% to 68% during inference step, which reduces 37.89% MAC with negligible accuracy drop on MS-COCO. Moreover, experimental results also show similar trends in heavy networks such as VGG and RetinaNet with ResNet101, and an additional dataset, PASCAL VOC. The code will be released.

## 1. Introduction

In recent years, we have witnessed the dramatic advancement and the success of deep learning. It has brought a great leap in the field of computer vision such as image classification [19, 25, 47] and object detection [28, 40]. The impact is not limited to the research society. Industries are already using deep learning for the development of artificial intelligence (AI) softwares and services such as autonomous driving, surveillance system, virtual assistant and health-care.

Training and running a deep learning model requires a large amount of computation power. It limits the scalability

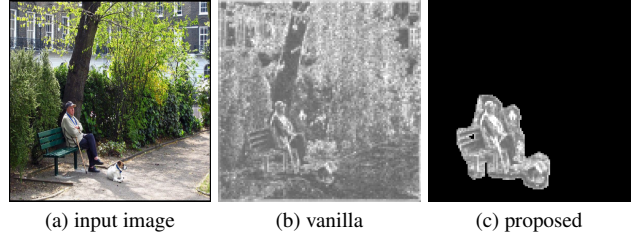


Figure 1. Comparison of generated feature maps; (a) input image, (b) feature map generated by a modern object detection model, (c) the proposed model's feature map. Feature maps are extracted from the end of the MobileNetV2's bottleneck block 2(1/4 level feature) and the absolute value of each pixel is averaged across channels.

and applicability of deep learning, especially for resource-constraint environments. To overcome this problem, substantial efforts are invested to increase the efficiency of deep learning models both in hardware and software aspects. To improve the performance in the deep neural networks, hardware designs for dealing with zero values [24], handling sparsity and high-precision outliers [36], on-chip convolutional neural network (CNN) models [2, 45] and specialized accelerators [30, 34] have been proposed. In the perspective of software acceleration, it includes light-weight network design [20, 39, 43], network pruning [12, 16] and network quantization [8, 23].

Object detection (OD) is one of the most popular applications in the field of computer vision. While a lot of efforts have been invested in developing efficient OD networks, state-of-the-art models still require huge computational resources. Therefore, practitioners are often forced to choose a suitable feature extractor (*a.k.a.* backbone network), which has higher accuracy (*e.g.* ResNet101) or faster speed (*e.g.* MobileNet), depending on the amount of expendable resources on a target environment.

In this paper, we propose an objectness-aware object detection method which processes only part of an input image where objects are likely to exist, which we call *foreground regions*. This approach is motivated by the observation that most feature map computations that occur in feature extraction network will be eventually discarded in anchor head

\*Corresponding author

†Equal contribution

network. To mitigate this phenomenon, we build a light-weight objectness mask generation (OMG) network which creates a binary mask that distinguishes foreground regions from background areas. This binary mask is then multiplied with a feature map before every convolution layer in an OD network. Sparse convolution can boost inference speed by circumventing unnecessary computation with little overhead on these zero-valued regions. Figure 1 shows a sample image (a) and feature maps generated by a modern OD model (b) and the objectness-aware OD model (c).

In experiments, we show that the proposed method effectively increases the number of zero values during forward pass with ReLU activation. For example, the computational cost of the original MobileNetV2-SSDLite [43] is 2.17 GMAC and its *approximated GMAC* ( $GMAC^*$ )<sup>1</sup> on the MS-COCO [27] validation dataset is 1.61 because of zero activation by ReLU. When the proposed method is applied,  $GMAC^*$  drops to 1.00 including OMG network. We found that this result is also consistent with heavy networks (VGG [46] and RetinaNet with ResNet101 [26]) and a different dataset (PASCAL VOC [9]). In addition, models using the proposed method achieve comparable detection accuracy to their original counterparts.

The main contributions of this paper are three-fold: **(i)** a novel object detection framework that accelerates inference speed by sparsifying activations, not model parameters [12, 15, 16, 29], **(ii)** an end-to-end model architecture to incorporate the OMG network into a modern OD model and **(iii)** an experimental result that shows training with only foreground region is not harmful, even better with a large margin if fine-grained masks such as ground-truth (GT) are provided.

## 2. Related Work

Traditional object detection methods and OverFeat [44], a deep learning approach, are based on the sliding window algorithm. To reduce the computational cost spent on searching the entire region with the sliding window manner, proposal-based two-stage R-CNN series have been proposed [13, 18, 40]. It successfully reduces the number of candidates for the background region, however, it still requires lots of computing resources to generate proposals. In the one-stage detectors such as SSD [28] and YOLO [39], the features of the convolutional backbone network are fed into subnetworks for object classification and bounding box regression. These one-stage detectors aim to be more efficient by directly classifying the pre-defined anchors and refining them using CNNs without the proposal generation step. However, it still requires to compute all of anchor candidates.

<sup>1</sup>GMAC\* calculates the computational cost with only non-zero activations. See Equation 3 and 4 for detailed explanation.

Semantic segmentation [7, 9, 27] is a task that classifies every pixel in an input image as one of pre-defined semantic classes. Most previous work on this task [5, 31, 37, 41] utilize both high-level information on a large receptive field to recognize objects of complex shapes and low-level features to keep their spatial details. For example, the seminal fully convolutional network model [31] uses many convolutional and pooling layers to distill abstract information from an input image and bilinear up-sampling and skip-connections from lower layers to restore spatial details. PSPNet [53] uses a pyramid pooling method to incorporate global context information. Two or multi-branch systems [38, 52] are popular that process an input image of multiple scales in parallel and fuse their feature maps at the end. However, the ultimate goal of this task is to generate a fine-grained segmentation map, which is different from our purpose that needs to build a coarse-grained binary mask as fast as possible. Saliency detection [6, 21, 32] is a similar task to semantic segmentation, except that salient areas are detected by pre-defined metrics not by training data.

Accelerating neural networks can be tackled in various ways. A straight-forward approach is to design efficient networks, manually [20, 43] or automatically [22]. From the opposite direction, we can train a heavy network and reduce model size by pruning insignificant parameters using network pruning techniques [12, 15, 16, 29]. These two approaches inevitably reduce network capacity and aggressive pruning suffers from accuracy drop. Another approach is to use quantization method [3, 8, 23]. Computational costs rapidly decrease when low-bit precision data types are used for weights and activations. Data sparsity can be exploited to increase the efficiency of neural networks. For example, hardware/software-accelerated sparse convolution mechanism [14, 35] greatly reduces the computational cost if weights or activations are very sparse. Several works [51, 11, 48] have proposed to dynamically scale computation through cascade or early termination. Zhang *et al.* [51] proposed cascade face detection which reduces face candidates by rejecting easy negatives in the early stage. Michael *et al.* [11] proposed a method that adaptively determines after which layer to stop computation. These approaches work effectively when the background is simple or not confused with the foreground. However, complex inputs require almost entire computation time, while the proposed method computes object region only.

## 3. Approach

The objectness-aware object detection model consists of two modules: OMG network and OD network. In Section 3.1, we illustrate the network architecture of the proposed model and its high level workflow. Section 3.2 describes OMG network and Section 3.3 explains how to integrate these two networks into the end-to-end model in detail.

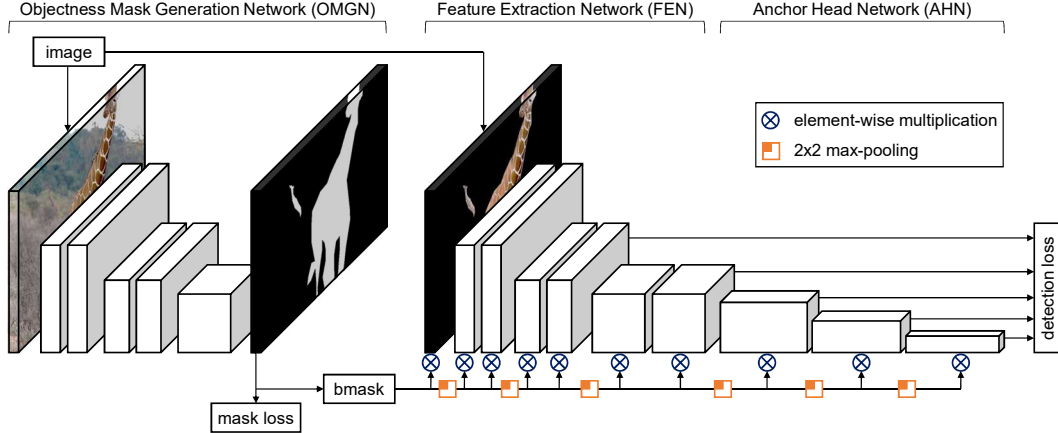


Figure 2. An illustrative view of our method for SSD. We incorporate an OMG network in front of a modern object detector. An input image is first fed into the objectness mask generator and it produces a binary mask (*bmask*). Then, the output feature map from each layer in the object detector (FEN+AHN) is multiplied with the mask to zero out the background region.

### 3.1. Objectness-aware Object Detection

In this study, we use Single Shot MultiBox Detector (SSD) [28] as a baseline OD framework. SSD consists of two main sub-modules: feature extraction network (FEN) and anchor head network (AHN). The feature map located at each anchor position is fed into AHN to determine the object class as well as localize its bounding box.

The proposed objectness-aware OD model integrates an OMG network in front of the baseline OD network as shown in Figure 2. An input image and all input features to convolutional layers of the OD network are now masked with a binary objectness mask, which zeros out pixel values in the background area. This masking operation is implemented as an element-wise multiplication layer denoted as  $\otimes$  symbol in the above figure. Also note that when the shape of a feature map changes due to the operations such as pooling and strided convolution, a max-pooling is applied to the mask so that its shape always matches that of the corresponding feature map.

The following section introduces our OMG method in detail. We also investigate other methods for objectness mask generation and present experimental results in 4.4.

### 3.2. Objectness Mask Generation

The OMG network takes an input image and generates a binary mask where background pixels have the value of zero and foreground pixels have the value of one. This task, classifying every pixel in an image as one of two classes, can be thought of as a simplified version of semantic segmentation [5, 31, 37, 38, 41, 52, 53]. The shape of an objectness mask can be an arbitrary shape, like a segmentation mask, or a box depending on the availability of annotation data. We adopted Fast-SCNN [38] as our OMG network because it is a fast and light-weight semantic segmentation model. In addition, it is a fully convolutional network so that we can

easily control its computational cost by changing the input image size. In Figure 2, the OMG network is shown in front of the OD network.

The purpose of OMG, however, is not identical to that of semantic segmentation. For example, misclassification of the foreground area results in a more serious impact than the opposite, because the objects inside that region will be lost in the OD step. In addition, even for a relatively large object, an OD model may experience difficulty in the regression of a bounding box position if the boundary areas (*e.g.* arms or legs of a person) are lost. Various methods are applied to emphasize the correct detection of foreground regions such as hard negative mining [10, 26, 28], cost-sensitive learning [1] and data pre-processing with dilation [17]. In Section 4.4.1, we explain details of these methods and analyze their effects on the mask generation.

### 3.3. End-to-end Network

We incorporate OMG and OD networks into an end-to-end model since it accelerates the performance and improves the accuracy by directly optimizing two networks for the final goal. However, it introduces a unique problem in the training process. The OMG network generates one of two discrete values, zero and one, for each input pixel by *argmax* function. Because *argmax* function is non-differentiable and the gradient is almost always zero, training the end-to-end model with the standard back-propagation is impossible.

There are two solutions we investigated to overcome this problem. The first option is to use the soft-version of *argmax* function,

$$\text{soft-argmax}(x) = \sum_i \frac{e^{\beta x_i}}{\sum_j e^{\beta x_j}} i, \quad (1)$$

where  $i$  is a class label and  $\beta$  is a hyper-parameter that deter-

mines the shape of the resulting distribution. We use  $\beta = 5$  in all experiments. After training, this *soft-argmax* function is replaced with *argmax*. While this approach allows us to train the end-to-end model, the discrepancy between two activation functions yields an AP drop.

The second solution is to use the surrogate gradient (SG) method [3, 23, 50]. This method uses a proxy derivative function for the backward pass that approximates the direction of the original activation function’s gradient. We use

$$\text{sg-argmax}(x) = \begin{cases} \text{argmax}(x) & \text{for forward} \\ \text{soft-argmax}(x) & \text{for backward} \end{cases} \quad (2)$$

that has differentiable and non-trivial gradient values suitable for back-propagation. This technique has been widely used in training quantized neural networks where activations are piece-wise constant functions and shown successful results empirically. In addition, a recent study [50] also shows theoretical evidence that, when a proper proxy derivative is chosen, the training process converges near the original local minima.

## 4. Experiments

In Section 4.1, 4.2 and 4.3, we explain terminologies, datasets and evaluation metrics and implementation details used across experiments. Then, we perform experiments in two different settings, a pipeline two-stage model and an end-to-end model, in Section 4.4 and 4.5.

The main goal of the first step is to investigate the best-known methods for training a good OMG model that plays a critical role in the proposed method. We evaluate OMG models trained with various techniques and compare their performance to other objectness mask generation methods.

In the second step, we integrate both OMG and OD networks into a single end-to-end model to explicitly guide the training process in the direction of improving the final object detection task performance. Evaluation results with three types of networks and two datasets are reported.

### 4.1. Preliminary

A convolution layer consists of a triplet  $\langle X_i, X_o, W \rangle$ , where  $X_i$  and  $X_o$  correspond to the input and output activation tensors, respectively, and  $W$  corresponds to the set of convolution kernels. Each activation tensor is a three-dimensional tensor of size  $w \times h \times c$ , where  $w$ ,  $h$  and  $c$  represent the tensor width, height, and depth, respectively. For convenience, the dimensions of  $X_i$  and  $X_o$  are denoted by  $[w_i \times h_i \times c_i]$  and  $[w_o \times h_o \times c_o]$ . The set of convolution kernels  $W$  is denoted by a four-dimensional tensor  $[k \times k \times c_i \times c_o]$ , where  $k$  is the kernel width and height. The kernel width and height are not necessarily equal, but it is common practice in most conventional CNNs to take

them. Given the above notation, the number of multiply-accumulate (MAC) operations for a single convolution layer is defined as

$$\text{MAC} = \frac{(w_i \times h_i) \times (k \times k) \times c_i \times c_o}{(s \times s)}, \quad (3)$$

where the  $s$  is stride for convolution kernel and the padding is omitted for simplicity’s sake. To calculate the MAC considering the zeros in activation tensor, we define approximated MAC as

$$\text{MAC}^* = \frac{(w_i \times h_i - z_i) \times (k \times k) \times c_i \times c_o}{(s \times s)}, \quad (4)$$

where the  $z_i$  is the number of zeros in  $X_i$  tensor. Since  $\text{MAC}^*$  approximates the MAC only considering the sparsity in activation tensor, the practical MAC can be reduced further if it also considers zero values in convolution kernels  $W$ , which can be maximized with network pruning [15]. We use the above notations throughout this paper.

### 4.2. Dataset and Evaluation Metrics

Our experiments are performed on two benchmark datasets: MS-COCO [27] and PASCAL VOC [9].

**MS-COCO** contains bounding box and instance segmentation annotations for 80 categories and 115k images for training (*train-2017*), 5k for validation (*val-2017*) and 20k for testing without annotations (*test-dev*). We train models on *train-2017*, report ablation studies on *val-2017* and evaluate final performance on *test-dev*. The main evaluation metric is Average Precision (AP) that averages AP across IoU thresholds from 0.50 to 0.95 with an interval of 0.05. Additionally, AP can be used to evaluate the performance under different object scales, including small objects ( $area < 32^2$ ), medium objects ( $32^2 < area < 96^2$ ) and large objects ( $area > 96^2$ ).

**PASCAL VOC** has bounding box annotations for 20 categories. VOC2007 dataset contains 10k images for train, val and test and VOC2012 dataset has 11k images for train and val. We train models on VOC2007 and VOC2012 *trainval* sets, and report results on VOC2007 *test* set. Similar to the evaluation metrics used in the MS-COCO benchmark, we report the mean AP (mAP) averaged over all object categories with the IoU threshold 0.5.

### 4.3. Implementation Details

For fair comparisons, all experiments are implemented based on publicly accessible softwares, MMDetection [4] and Fast-SCNN [49], using PyTorch. The backbone networks used in our experiments are also publicly available.

In the pipeline approach, OMG models are trained for 160 epochs with one GPU and 64 batch size. Initial learning rate is set to 0.02 with the polynomial learning rate decay, which decreases the learning rate with  $lr = lr_{initial} * (1 - \frac{epoch}{160})^{0.9}$

$(1 - epoch_{current}/epoch_{max})^2$ . Images of the training dataset are resized to fit their shorter edges to 640 pixels and randomly cropped into 320x320 patches. OD models are trained with two GPUs (24 images per GPU) for 24 epochs with an initial learning rate of 0.02, decreased by a factor of 10 after 16 and 22 epochs.

To train end-to-end models, we use four GPUs (12 images per GPU) for 36 epochs with an initial learning rate of 0.02, decreased by a factor of 10 after 24 and 33 epochs. The network backbones for OD are pre-trained on the ImageNet [42] and then fine-tuned on the detection dataset. Because the OMG network is integrated into the OD network, its training scheme such as training epochs, learning rate, and data augmentation now follows that of OD models. We increased the number of training epochs 1.5 times for the end-to-end models because the OMG network is not pre-trained at all and it affects OD network negatively at the beginning of the training. All other hyper-parameters follow the settings in MMDetection [4] and Fast-SCNN [49] if not mentioned in particular.

#### 4.4. Pipeline Approach

Objectness masks can be generated in many ways. In this experiment, we build a pipeline system and runs a series of experiments using various mask generation methods including random mask generation, spectral residual saliency detection method [21] and the proposed OMG method. We also use GT instance and bounding-box masks to investigate the upper-bound accuracy of the proposed approach. In the following section, we explain the proposed OMG method in detail. The other methods will be described in 4.4.2.

##### 4.4.1 Objectness Mask Generation

To make an OMG model better recognize foreground regions, we use the following three techniques.

**Mask Dilation (MD)** expands the boundary of GT objectness masks using dilation [17] algorithm. When an OMG model trained with dilated GT masks, it detects small and thin foreground areas better. In Figure 3, we can see that MD remarkably improves instance recall of predicted objectness masks at the cost of foreground ratio (*FG-ratio*).

**Online Hard-Negative Example Mining (OHNEM)** is a sampling method that selectively uses negative examples having the highest losses. Because only a small fraction of the entire region is foreground in many images, the baseline model tends to predict background rather than foreground. OHNEM can mitigate this problem by using negative examples proportional to the number of positive examples.

**Loss Re-Weighting (LW)** is a cost-sensitive learning method. To emphasize the correct prediction of foreground areas, we give higher loss when they are misclassified. We investigated how these methods influence the proposed

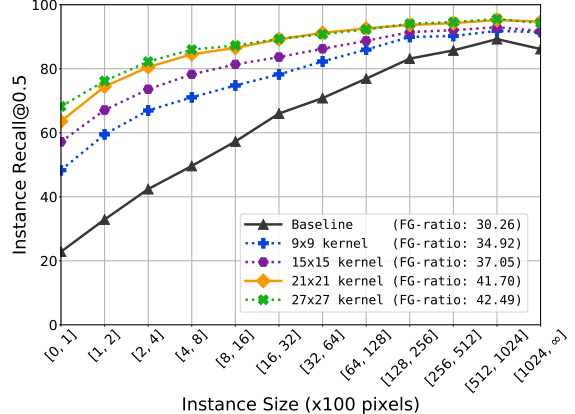


Figure 3. The effect of mask dilation on MS-COCO *val-2017* dataset. Note: X-axis shows the size of instances in specific ranges. Y-axis shows instance recall with the threshold 0.5 (if more than the half of the pixels of an instance is classified as foreground, that instance is considered as true positive).

Method	Param	Instance Recall@0.5	FG-ratio
Baseline		60.02	30.26
MD	9	75.54	34.92
	15	80.67	37.05
	21	85.73	41.70
	27	86.68	42.49
OHNEM	1:3	66.54	32.62
	1:1	73.97	38.67
	2:1	85.98	55.02
LW	2:1	78.46	37.79
	3:1	85.75	42.23
ALL	21, 1:3, 3:1	96.07	50.74

Table 1. The effect of MD, OHNEM, LW and their combination (ALL) on MS-COCO *val-2017* dataset. *Param* column indicates the kernel size, positive and negative sample ratio, and loss re-weighting values for positive and negative classes, respectively.

OMG method.

Table 1 summarizes the results. All of these methods improve instance recall at the cost of increasing FG-ratio. We also choose the combination of these three methods (*ALL*) that maximizes instance recall while keeping the FG-ratio around 50% and used for the E2E system.

##### 4.4.2 Object Detection

In order to compare detection results using various objectness masks, we use MobileNetV2-SSDLite [43] as our baseline OD model, pre-trained on the ImageNet [42] dataset. Note that all convolution layers in SSD prediction layers are replaced with depthwise separable convolutions (*a.k.a.* SSDLite). All models are fine-tuned on the MS-COCO *train-2017* dataset with input image resolution of 512x512. We perform evaluation on the *val-2017* and report the results in Table 2. All of these experiments except vanilla model use both images and static objectness masks.

mask	FG-ratio (%)	zeros%	zeros% by mask	GMAC*	AP	AP <sub>50</sub>	AP <sub>75</sub>	AP <sub>S</sub>	AP <sub>M</sub>	AP <sub>L</sub>
vanilla	100	36.47	N/A	1.61	22.6	40.3	22.7	6.7	23.7	36.5
GT mask	30	81.66	66.64	0.54	35.8	51.3	38.5	15.9	38.8	48.5
GT box mask	43	72.56	54.03	0.74	37.6	51.3	40.0	15.9	40.8	53.2
SR mask	50	66.50	43.45	0.97	16.8	32.2	15.7	4.5	18.0	26.3
random mask	30	47.78	9.90	1.51	17.5	32.0	17.1	3.2	17.0	30.3
random mask	50	42.92	3.80	1.54	18.6	34.0	18.2	3.8	18.8	31.5
OMG mask	51	69.02	46.39	0.88	20.4	36.5	20.4	4.7	20.6	34.6

Table 2. Comparison of different static objectness mask for objectness-aware object detection on MS-COCO *val-2017*.

**Vanilla.** The vanilla model has 36.47% zero values in the entire feature maps because of the ReLU activation [33]. Similar to the reported performance in the original paper [43], it achieves 22.6 AP as shown in Table 2.

**Instance GT Mask.** To understand the effect of using only foreground region for object detection and its upper-bound performance, we trained and evaluated a model using the GT instance segmentation annotation as objectness masks. Without bells and whistles, it achieves 35.8 AP which is 13.2 points higher than the vanilla model. It implies that background information is not necessarily essential and high-quality masks can help to achieve better accuracy for object detection. In terms of computational cost, it requires only 33.5% (0.54 GMAC\*) of the vanilla model (1.61 GMAC\*).

**Box GT Mask.** Since building an instance segmentation dataset is time-consuming and costly work, not all datasets have instance segmentation annotation. Assuming that a given dataset has only bounding-box annotation, we trained a model to examine the upper-bound performance of the proposed method. It achieves the highest AP (37.6) among all models, even higher than the instance GT mask model. We speculate that the model performs better because the shape of objectness masks are identical to that of target bounding boxes. However, its average FG-ratio is 13% higher than that of the instance GT mask model.

**SR Mask.** Spectral residual method [21] is one of saliency detection algorithms. It identifies specific areas of an image where unusual frequency information resides based on the natural image statistics. This method doesn't need a training dataset and runs very fast. We trained a model using objectness masks generated with this method. To limit the average FG-ratio under 50%, the threshold 0.08 is used. This model achieves the lowest AP among all models, even worse than the models trained with random masks. It results from the fact that salient areas don't necessarily correspond to the regions where target objects exist.

**Random Mask.** One of the simplest approaches to reduce MAC\* is to use random objectness masks. We trained two models with random masks generated by using a salt-and-pepper noise pattern with targeted FG-ratios, 30%, and 50%. Compared to the baseline model, these models yield noticeable accuracy drop, 5.1 and 4.0 points, respectively.

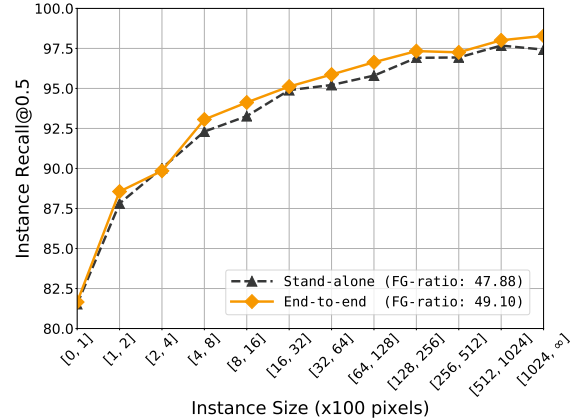


Figure 4. Comparison of instance recall of OMG masks generated from the stand-alone OMG model and the end-to-end model. These models use the same training and inference schemes such as input image size and data augmentation methods.

OMG input	E2E	GMAC*			COCO		
		sum	OMG	OD	AP	AP <sub>50</sub>	AP <sub>75</sub>
256 <sup>2</sup>	✗	0.95	0.14	0.81	20.2	36.1	20.4
256 <sup>2</sup>	✓	1.01	0.14	0.87	21.4	37.6	21.5
512 <sup>2</sup>	✓	1.39	0.56	0.83	21.6	37.8	21.7

Table 3. Results of different combinations of the OMG network.

However, the biggest problem is the GMAC\* values. While the average FG-ratios are 30% and 50%, their GMAC\* values aren't much different from that of the vanilla model because random background pixels mostly disappear when the first max-pooling is applied to reduce mask shape.

**OMG Mask.** We trained a model with the objectness masks generated by the proposed OMG method explained in 3.2. Unlike the training process, raw input images are used without resizing for mask generation in the same manner as *SR Mask* and *Random Mask* models. This is different from our end-to-end model that uses resized input images. Although it yields 2.2 lower AP compared with the vanilla model, its GMAC\* is almost half of it. In the following section, we present the experiments using the end-to-end model that mitigates this accuracy gap by training OMG and OD as a single model.

	width multiplier	image	mask GT	SG	GMAC	GMAC*	AP	AP <sub>50</sub>	AP <sub>75</sub>	AP <sub>S</sub>	AP <sub>M</sub>	AP <sub>L</sub>
vanilla	0.75	512 <sup>2</sup>	N/A	N/A	1.61	1.21	20.0	36.5	19.4	5.0	20.0	32.6
	0.5	512 <sup>2</sup>			0.95	0.69	15.9	30.0	15.1	3.1	15.4	27.5
	1.0	416 <sup>2</sup>			1.44	1.07	20.1	37.0	19.4	4.8	19.8	33.6
	1.0	352 <sup>2</sup>			1.03	0.77	17.8	33.8	16.9	4.0	17.6	29.0
ours	1.0	512 <sup>2</sup>	instance	✗	2.37	1.26	21.2	37.9	21.3	5.0	21.8	35.5
			instance	✓		1.01	21.4	37.6	21.5	5.6	21.8	35.9
			box	✓		1.17	22.0	38.3	22.2	5.6	22.7	36.4
ours <sup>+</sup>	1.0	512 <sup>2</sup>	instance	✓	2.37	1.00	22.2	38.4	22.7	5.8	22.6	37.5

Table 4. Comparison of the proposed method to the other MAC-reduction approaches on MS-COCO *val-2017*

#### 4.5. End-to-end Approach

In the case of MobileNetV2, we use an input image resolution of 256<sup>2</sup> for OMG and 512<sup>2</sup> for OD to reduce the computational cost for mask generation. The generated mask is re-scaled to 512<sup>2</sup> by bilinear up-sampling before *argmax*. The computational cost of OMG network is only 10% of MobileNetV2-SSDLite.

To compare the quality of objectness masks between pipeline and end-to-end approaches, we evaluate two models with the same configuration except for the connection of two networks. As shown in Figure 4, the masks generated from the end-to-end model exhibit higher instance recall than those generated by the pipeline model for all instance sizes. This experiment result shows that additional losses back-propagated from the OD network to the OMG network contribute to the high-quality mask generation.

Our end-to-end model also achieves 1.2 points higher AP than the pipeline model as shown in Table 3. It implies that improved mask generation by OD losses also helps to enhance object detection performance. In addition, we tried a larger input image size (512<sup>2</sup>) for the OMG network. It improves 0.2 points in AP, but increases GMAC<sub>OMG</sub>\* four times from 0.14 to 0.56.

Figure 5 shows the average ratio of zero values at each feature map blocks for MS-COCO validation set compare to the vanilla model. Although ReLU activation already made activation very sparse (36.47% of feature maps are zero in the vanilla model), the proposed method pushes this number to 68.10%. This leads to the reduction of computational cost by 0.61 GMAC\*, 37.89% decrease.

In Table 4, we compare the proposed method with other MAC-reduction approaches using low resolution input images and small capacity networks (with *width multiplier* option of MobileNetV2). As shown in Table 4, our models using the proposed method always outperform the vanilla models, even if some of them have larger GMAC\* than ours. In addition, the use of SG method (Eq. 2) improves both AP and GMAC\* than *soft-argmax* method (Eq. 1).

In addition, we trained the model using instance GT mask once again with the same training scheme to see if it has converged completely. The trained model, shown as *ours<sup>+</sup>* in Table 4, achieved 22.2 points AP (+0.8) and 1.00

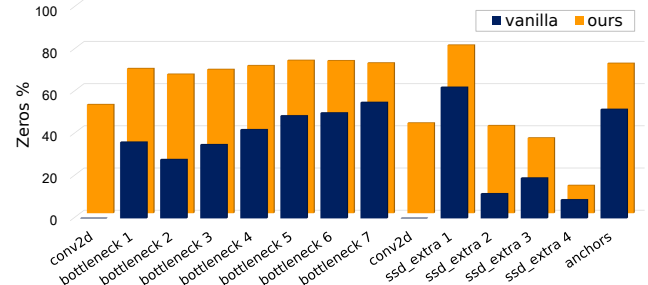


Figure 5. The proportion of zero values at each feature map blocks in the object detection network (SSDLite512 with MobileNetV2); our method largely increases zero values for the entire feature maps on MS-COCO *val-2017*.

network	method	GMAC	GMAC*	AP	AP <sub>50</sub>	AP <sub>75</sub>
VGG	vanilla	86.70	37.38	29.5	48.8	30.9
	GT mask	86.70	11.85	44.5	61.5	48.5
	ours	87.53	23.91	27.5	46.2	28.5
RetinaNet w/ R101	vanilla	135.02	53.56	37.6	57.6	40.1
	GT mask	135.02	18.24	51.3	67.1	55.1
	ours	137.89	37.06	36.5	56.3	39.0

Table 5. Evaluation results of the end-to-end model with heavy backbones on MS-COCO *val-2017*. The input image resolution of 512x512 and 1216x800 is used for VGG and RetinaNet, respectively.

network	method	GMAC	GMAC*	AP	AP <sub>50</sub>	AP <sub>75</sub>
MobileNet	vanilla	2.17	1.61	22.8	40.6	22.8
	ours	2.37	1.00	21.5	37.9	21.4
VGG	vanilla	86.70	37.35	29.6	49.0	31.2
	ours	87.53	23.65	27.6	46.2	28.9
RetinaNet w/ R101	vanilla	135.02	53.52	38.0	58.5	40.9
	ours	137.89	36.70	36.7	56.9	39.4

Table 6. Evaluation results on MS-COCO *test-dev*

method	FG-ratio (%)	GMAC	GMAC*	mAP
vanilla	100	1.82	1.39	74.0
GT box mask	44	1.82	0.67	80.1
ours	64	2.03	1.03	71.4

Table 7. Evaluation results on VOC2007 *test*

GMAC\* (-0.01). This result shows that training the end-to-end model requires additional hyper-parameter tuning.

Figure 6 shows sample images with their feature maps

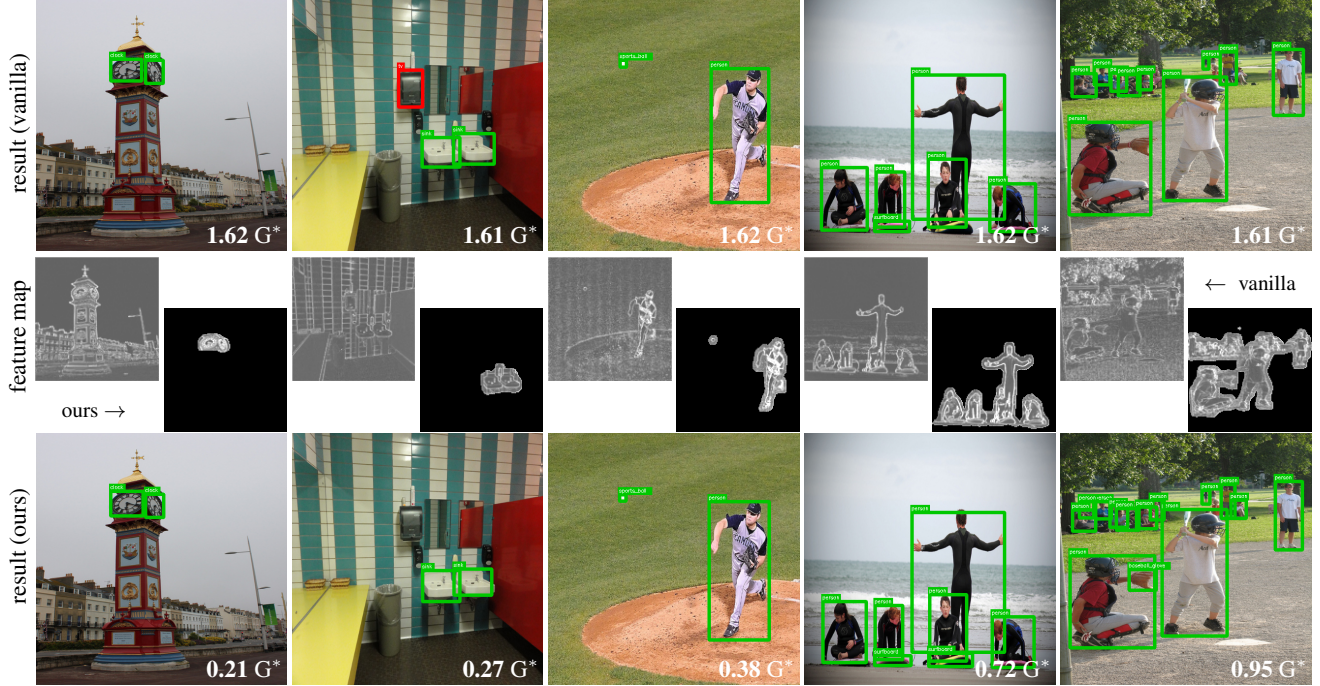


Figure 6. Qualitative comparison between the vanilla model and the proposed model(end-to-end). **Green** box represents true positive, whereas **red** box indicates a false positive. ( $G^*$  stands for GMAC\* and it includes both OMG and OD network’s computations)

and detection results for the vanilla model and the proposed model. To visualize a feature map, we average absolute feature values across channels at the end of bottleneck block 2 which has  $128^2$  size. As shown in the second row, our method generates a feature map where only a small portion is the foreground region. As a result, MAC\* value for each image is very small as shown in the right bottom area of that image. These results tell us that the proposed model is going to operate with very low MAC\* in many practical applications such as autonomous driving or surveillance camera. In addition, the objectness mask often filters out false-positives of the vanilla model, as shown in the second column image.

To evaluate the generality of the proposed method, we have experimented with heavy backbone networks. Table 5 shows the MAC\* reduction comparing to their vanilla models. Our approaches only use about 64% of vanilla MAC\* with a little drop of AP (2.0 and 1.1 for VGG and RetinaNet, respectively). Compare to the original MAC, our approaches use only 28% MAC.

Lastly, Table 6 reports the evaluation result on MS-COCO *test-dev*. The result of the three models is almost consistent with the experimental results on *val-2017*. The evaluation result on VOC2007 *test* in Table 7 also shows the same trend even if the dataset is changed.

## 5. Conclusion

In this paper, we have presented a novel object detection model that accelerates detection performance by skipping

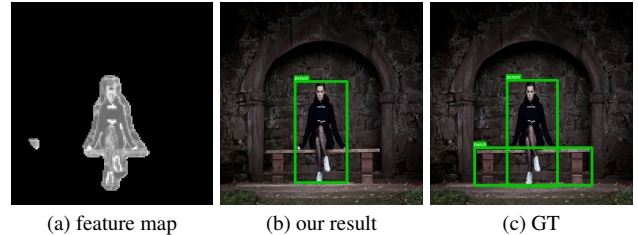


Figure 7. Limitation of the proposed method. OD fails to detect target objects if OMG generates an incomplete mask.

the calculation on the background region with sparse convolution. We use an OMG network to accomplish this purpose and integrate them in an end-to-end manner. The experimental results with three popular network architectures and two datasets have shown that the proposed method can greatly reduce the computational cost while keeping comparable detection accuracy compared to the original models. In addition, experiments with GT masks have shown that there is a lot of room for improvement in terms of both accuracy and speed.

However, our method constraints the detectable performance by the instance recall of the OMG. For example, the bench object could not be detected since OMG doesn’t provide this region as a foreground, as shown in Figure 7.

For future work, we plan to evaluate the effect of state-of-the-art segmentation algorithms, which may improve object detection accuracy.

## References

- [1] Aida Ali, Siti Mariyam Shamsuddin, and Anca L. Ralescu. Classification with class imbalance problem: A review. *International Journal of Advances in Soft Computing and its Application*, 7(3):176–204, 2015. 3
- [2] Daniel Bankman, Lita Yang, Bert Moons, Marian Verhelst, and Boris Murmann. An always-on  $3.8\mu\text{J}/86\%$  CIFAR-10 mixed-signal binary CNN processor with all memory on chip in 28nm CMOS. *Journal of Solid-State Circuits*, 54(1):158–172, 2019. 1
- [3] Zhaowei Cai, Xiaodong He, Jian Sun, and Nuno Vasconcelos. Deep learning with low precision by half-wave gaussian quantization. In *Computer Vision and Pattern Recognition*, pages 5406–5414, 2017. 2, 4
- [4] Kai Chen, Jiaqi Wang, Jiangmiao Pang, Yuhang Cao, Yu Xiong, Xiaoxiao Li, Shuyang Sun, Wansen Feng, Ziwei Liu, Jiarui Xu, Zheng Zhang, Dazhi Cheng, Chenchen Zhu, Tianheng Cheng, Qijie Zhao, Buyu Li, Xin Lu, Rui Zhu, Yue Wu, Jifeng Dai, Jingdong Wang, Jianping Shi, Wanli Ouyang, Chen Change Loy, and Dahu Lin. MMDetection: Open MMLab detection toolbox and benchmark. <https://github.com/open-mmlab/mmdetection>, 2019. 4, 5
- [5] Liang-Chieh Chen, George Papandreou, Iasonas Kokkinos, Kevin Murphy, and Alan L. Yuille. DeepLab: Semantic image segmentation with deep convolutional nets, atrous convolution, and fully connected CRFs. *IEEE Transactions on Pattern Analysis and Machine Intelligence*, 40(4):834–848, 2018. 2, 3
- [6] Ming-Ming Cheng, Ziming Zhang, Wen-Yan Lin, and Philip H. S. Torr. BING: binarized normed gradients for objectness estimation at 300fps. In *Computer Vision and Pattern Recognition*, pages 3286–3293, 2014. 2
- [7] Marius Cordts, Mohamed Omran, Sebastian Ramos, Timo Rehfeld, Markus Enzweiler, Rodrigo Benenson, Uwe Franke, Stefan Roth, and Bernt Schiele. The Cityscapes dataset for semantic urban scene understanding. In *Computer Vision and Pattern Recognition*, pages 3213–3223, 2016. 2
- [8] Matthieu Courbariaux, Yoshua Bengio, and Jean-Pierre David. BinaryConnect: Training deep neural networks with binary weights during propagations. In *Neural Information Processing Systems*, pages 3123–3131, 2015. 1, 2
- [9] Mark Everingham, S. M. Ali Eslami, Luc Van Gool, Christopher K. I. Williams, John M. Winn, and Andrew Zisserman. The PASCAL visual object classes challenge: A retrospective. *International Journal of Computer Vision*, 111(1):98–136, 2015. 2, 4
- [10] Pedro F. Felzenszwalb, Ross B. Girshick, and David A. McAllester. Cascade object detection with deformable part models. In *Computer Vision and Pattern Recognition*, pages 2241–2248, 2010. 3
- [11] Michael Figurnov, Maxwell D. Collins, Yukun Zhu, Li Zhang, Jonathan Huang, Dmitry P. Vetrov, and Ruslan Salakhutdinov. Spatially adaptive computation time for residual networks. In *Computer Vision and Pattern Recognition*, pages 1790–1799, 2017. 2
- [12] Jonathan Frankle and Michael Carbin. The lottery ticket hypothesis: Finding sparse, trainable neural networks. In *International Conference on Learning Representations*, 2019. 1, 2
- [13] Ross B. Girshick. Fast R-CNN. In *International Conference on Computer Vision*, pages 1440–1448, 2015. 2
- [14] Benjamin Graham, Martin Engelcke, and Laurens van der Maaten. 3D semantic segmentation with submanifold sparse convolutional networks. In *Computer Vision and Pattern Recognition*, pages 9224–9232, 2018. 2
- [15] Song Han, Huizi Mao, and William J. Dally. Deep compression: Compressing deep neural network with pruning, trained quantization and huffman coding. In *International Conference on Learning Representations*, 2016. 2, 4
- [16] Song Han, Jeff Pool, John Tran, and William J. Dally. Learning both weights and connections for efficient neural network. In *Neural Information Processing Systems*, pages 1135–1143, 2015. 1, 2
- [17] Robert M. Haralick, Stanley R. Sternberg, and Xinhua Zhuang. Image analysis using mathematical morphology. *IEEE Transaction Pattern Analysis and Machine Intelligence*, 9(4):532–550, 1987. 3, 5
- [18] Kaiming He, Xiangyu Zhang, Shaoqing Ren, and Jian Sun. Spatial pyramid pooling in deep convolutional networks for visual recognition. *IEEE Transaction Pattern Analysis and Machine Intelligence*, 37(9):1904–1916, 2015. 2
- [19] Kaiming He, Xiangyu Zhang, Shaoqing Ren, and Jian Sun. Deep residual learning for image recognition. In *Computer Vision and Pattern Recognition*, pages 770–778, 2016. 1
- [20] Sanghoon Hong, Byungseok Roh, Kye-Hyeon Kim, Yeongjae Cheon, and Minje Park. PVANet: Lightweight deep neural networks for real-time object detection. In *International Workshop on Efficient Methods for Deep Neural Networks*, 2016. 1, 2
- [21] Xiaodi Hou and Liqing Zhang. Saliency detection: A spectral residual approach. In *Computer Vision and Pattern Recognition*, 2007. 2, 5, 6
- [22] Andrew Howard, Mark Sandler, Grace Chu, Liang-Chieh Chen, Bo Chen, Mingxing Tan, Weijun Wang, Yukun Zhu, Ruoming Pang, Vijay Vasudevan, Quoc V. Le, and Hartwig Adam. Searching for MobileNetV3. In *International Conference on Computer Vision*, October 2019. 2
- [23] Itay Hubara, Matthieu Courbariaux, Daniel Soudry, Ran El-Yaniv, and Yoshua Bengio. Binarized neural networks. In *Neural Information Processing Systems*, pages 4107–4115, 2016. 1, 2, 4
- [24] Dongyoung Kim, Junwhan Ahn, and Sungjoo Yoo. A novel zero weight/activation-aware hardware architecture of convolutional neural network. In *Design, Automation & Test in Europe Conference & Exhibition*, pages 1462–1467, 2017. 1
- [25] Alex Krizhevsky, Ilya Sutskever, and Geoffrey E. Hinton. ImageNet classification with deep convolutional neural networks. In *Neural Information Processing Systems*, pages 1106–1114, 2012. 1
- [26] Tsung-Yi Lin, Priya Goyal, Ross B. Girshick, Kaiming He, and Piotr Dollár. Focal loss for dense object detection. In *International Conference on Computer Vision*, pages 2999–3007, 2017. 2, 3

[27] Tsung-Yi Lin, Michael Maire, Serge J. Belongie, James Hays, Pietro Perona, Deva Ramanan, Piotr Dollár, and C. Lawrence Zitnick. Microsoft COCO: common objects in context. In *European Conference on Computer Vision*, pages 740–755, 2014. [2](#), [4](#)

[28] Wei Liu, Dragomir Anguelov, Dumitru Erhan, Christian Szegedy, Scott E. Reed, Cheng-Yang Fu, and Alexander C. Berg. SSD: single shot multibox detector. In *European Conference on Computer Vision*, pages 21–37, 2016. [1](#), [2](#), [3](#)

[29] Zhuang Liu, Mingjie Sun, Tinghui Zhou, Gao Huang, and Trevor Darrell. Rethinking the value of network pruning. In *International Conference on Learning Representations*, 2019. [2](#)

[30] Ivan Lobachev, Roman Maleryk, Svitlana Antoschuk, Denys Filiahin, and Mykhaylo Lobachev. Integration of neural networks into smart sensor networks. In *International Conference on Dependable Systems, Services and Technologies*, pages 544–548, May 2018. [1](#)

[31] Jonathan Long, Evan Shelhamer, and Trevor Darrell. Fully convolutional networks for semantic segmentation. In *Computer Vision and Pattern Recognition*, pages 3431–3440, 2015. [2](#), [3](#)

[32] Sebastian Montabone and Alvaro Soto. Human detection using a mobile platform and novel features derived from a visual saliency mechanism. *Journal of Image and Vision Computing*, 28(3):391–402, 2010. [2](#)

[33] Vinod Nair and Geoffrey E. Hinton. Rectified linear units improve restricted boltzmann machines. In *International Conference on Machine Learning*, pages 807–814, 2010. [6](#)

[34] Nashwan Adnan Othman and Ilhan Aydin. A new deep learning application based on Movidius NCS for embedded object detection and recognition. In *International Symposium on Multidisciplinary Studies and Innovative Technologies*, pages 1–5, October 2018. [1](#)

[35] Angshuman Parashar, Minsoo Rhu, Anurag Mukkara, Antonio Puglielli, Rangharajan Venkatesan, Brucek Khailany, Joel S. Emer, Stephen W. Keckler, and William J. Dally. SCNN: An accelerator for compressed-sparse convolutional neural networks. In *International Symposium on Computer Architecture*, pages 27–40, 2017. [2](#)

[36] Eunhyeok Park, Dongyoung Kim, and Sungjoo Yoo. Energy-efficient neural network accelerator based on outlier-aware low-precision computation. In *International Symposium on Computer Architecture*, pages 688–698, 2018. [1](#)

[37] Pedro H. O. Pinheiro and Ronan Collobert. Recurrent convolutional neural networks for scene labeling. In *International Conference on Machine Learning*, pages 82–90, 2014. [2](#), [3](#)

[38] Rudra P. K. Poudel, Stephan Liwicki, and Roberto Cipolla. Fast-SCNN: Fast semantic segmentation network. In *British Machine Vision Conference*, 2019. [2](#), [3](#)

[39] Joseph Redmon, Santosh Kumar Divvala, Ross B. Girshick, and Ali Farhadi. You only look once: Unified, real-time object detection. In *Computer Vision and Pattern Recognition*, pages 779–788, 2016. [1](#), [2](#)

[40] Shaoqing Ren, Kaiming He, Ross B. Girshick, and Jian Sun. Faster R-CNN: Towards real-time object detection with region proposal networks. In *Neural Information Processing Systems*, pages 91–99, 2015. [1](#), [2](#)

[41] Olaf Ronneberger, Philipp Fischer, and Thomas Brox. U-net: Convolutional networks for biomedical image segmentation. In *Medical Image Computing and Computer-Assisted Intervention*, pages 234–241, 2015. [2](#), [3](#)

[42] Olga Russakovsky, Jia Deng, Hao Su, Jonathan Krause, Sanjeev Satheesh, Sean Ma, Zhiheng Huang, Andrej Karpathy, Aditya Khosla, Michael S. Bernstein, Alexander C. Berg, and Fei-Fei Li. ImageNet large scale visual recognition challenge. *International Journal of Computer Vision*, 115(3):211–252, 2015. [5](#)

[43] Mark Sandler, Andrew G. Howard, Menglong Zhu, Andrey Zhmoginov, and Liang-Chieh Chen. MobileNetV2: Inverted residuals and linear bottlenecks. In *Computer Vision and Pattern Recognition*, pages 4510–4520, 2018. [1](#), [2](#), [5](#), [6](#)

[44] Pierre Sermanet, David Eigen, Xiang Zhang, Michaël Mathieu, Rob Fergus, and Yann LeCun. Overfeat: Integrated recognition, localization and detection using convolutional networks. In *International Conference on Learning Representations*, 2014. [2](#)

[45] Yongming Shen, Michael Ferdman, and Peter A. Milder. Escher: A CNN accelerator with flexible buffering to minimize off-chip transfer. In *International Symposium on Field-Programmable Custom Computing Machines*, pages 93–100, 2017. [1](#)

[46] Karen Simonyan and Andrew Zisserman. Very deep convolutional networks for large-scale image recognition. In *International Conference on Learning Representations*, 2015. [2](#)

[47] Christian Szegedy, Wei Liu, Yangqing Jia, Pierre Sermanet, Scott E. Reed, Dragomir Anguelov, Dumitru Erhan, Vincent Vanhoucke, and Andrew Rabinovich. Going deeper with convolutions. In *Computer Vision and Pattern Recognition*, pages 1–9, 2015. [1](#)

[48] Surat Teerapittayanon, Bradley McDanel, and H. T. Kung. BranchyNet: Fast inference via early exiting from deep neural networks. In *International Conference on Pattern Recognition*, pages 2464–2469, 2016. [2](#)

[49] Tramac. A pytorch implementation of fast-scnn: Fast semantic segmentation network. <https://github.com/Tramac/Fast-SCNN-pytorch>. [4](#), [5](#)

[50] Penghang Yin, Jiancheng Lyu, Shuai Zhang, Stanley J. Ossher, Yingyong Qi, and Jack Xin. Understanding straight-through estimator in training activation quantized neural nets. In *International Conference on Learning Representations*, 2019. [4](#)

[51] Kaipeng Zhang, Zhanpeng Zhang, Zhifeng Li, and Yu Qiao. Joint face detection and alignment using multitask cascaded convolutional networks. *IEEE Signal Processing Letters*, 23(10):1499–1503, Oct 2016. [2](#)

[52] Hengshuang Zhao, Xiaojuan Qi, Xiaoyong Shen, Jianping Shi, and Jiaya Jia. ICNet for real-time semantic segmentation on high-resolution images. In *European Conference on Computer Vision*, pages 418–434, 2018. [2](#), [3](#)

[53] Hengshuang Zhao, Jianping Shi, Xiaojuan Qi, Xiaogang Wang, and Jiaya Jia. Pyramid scene parsing network. In *Computer Vision and Pattern Recognition*, pages 6230–6239, 2017. [2](#), [3](#)